Please cite this article in press as: Paul et al., *FDXR* Mutations Cause Sensorial Neuropathies and Expand the Spectrum of Mitochondrial Fe-S-Synthesis Diseases, The American Journal of Human Genetics (2017), http://dx.doi.org/10.1016/j.ajhg.2017.09.007

REPORT

FDXR Mutations Cause Sensorial Neuropathies and Expand the Spectrum of Mitochondrial Fe-S-Synthesis Diseases

Antoine Paul,[1] Anthony Drecourt,[1] Floriane Petit,[1] Delphine Dupin Deguine,[2] Christelle Vasnier,[3] Myriam Oufadem,[1] Cécile Masson,[1] Crystel Bonnet,[4] Saber Masmoudi,[5] Isabelle Mosnier,[6] Laurence Mahieu,[7] Didier Bouccara,[6] Josseline Kaplan,[1] Georges Challe,[8] Christelle Domange,[9] Fanny Mochel,[10] Olivier Sterkers,[6] Sylvie Gerber,[1] Patrick Nitschke,[1] Christine Bole-Feysot,[1] Laurence Jonard,[11] Souad Gherbi,[12] Oriane Mercati,[12] Ines Ben Aissa,[12] Stanislas Lyonnet,[1,13] Agnès Rötig,[1] Agnès Delahodde,[3,14] and Sandrine Marlin[1,12,13,14,*]

Hearing loss and visual impairment in childhood have mostly genetic origins, some of them being related to sensorial neuronal defects. Here, we report on eight subjects from four independent families affected by auditory neuropathy and optic atrophy. Whole-exome sequencing revealed biallelic mutations in *FDXR* in affected subjects of each family. *FDXR* encodes the mitochondrial ferredoxin reductase, the sole human ferredoxin reductase implicated in the biosynthesis of iron-sulfur clusters (ISCs) and in heme formation. ISC proteins are involved in enzymatic catalysis, gene expression, and DNA replication and repair. We observed deregulated iron homeostasis in *FDXR* mutant fibroblasts and indirect evidence of mitochondrial iron overload. Functional complementation in a yeast strain in which *ARH1*, the human *FDXR* ortholog, was deleted established the pathogenicity of these mutations. These data highlight the wide clinical heterogeneity of mitochondrial disorders related to ISC synthesis.

Hearing loss and visual defects have mostly genetic origins. Several syndromes, including Usher (OMIM: 276903) and Wolfram syndromes (OMIM: 606201), are associated with hearing and visual impairments. Sensorial neuropathies are less frequent than cochlear and retinal defects. Auditory neuropathies (ANs) represent about 8% of congenital deafness,[1,2] and the prevalence of optic atrophy (OA) is 1/40,000.[3] The association between ANs and OA can be part of a multiorgan syndrome, usually implicating other neurologic systems. Examples include Friedreich ataxia (OMIM: 606829), Charcot-Marie-Tooth disease (OMIM: 159440), Brown-Vialetto-Van-Laere syndrome (OMIM: 614707), and Mohr-Tranebjaerg syndrome (OMIM: 304700). The AN-OA association is due to specific rare *OPA1* (OMIM: 605290) and *TMEM126A* (OMIM: 612988) mutations.[4,5] Interestingly, several of the implicated genes encode mitochondrial proteins.

Here, we report on eight subjects, two boys and six girls, from four different families (F1–F4) affected by AN and OA. The first clinical signs were observed during childhood or adolescence. The four families are from different origins (F1—Tunisia; F2—Algeria; F3—France; and F4—Azerbaijan and Russia). All parents were healthy, and there were no cases of sensorial defect in any relatives. Recurrence of the AN-OA was observed in two families, F1 and F4, with 2/5 and 2/4 of the children being affected, respectively (Figure 1, Table 1, and Supplemental Note). Consanguinity was noted only in family 1. All subjects were born at term, after normal pregnancy and delivery, with normal parameters. They all had normal psychomotor development except that subject 7 had a slight language delay; she spoke her first words at 2 years of age (Table 1 and Supplemental Note). For all subjects the diagnosis of AN was made on the basis of severe impaired auditory brainstem responses (ABRs), discrepancies between tonal and vocal audiometry, and the presence of otoacoustic emissions on both ears (Figure S1A). All subjects underwent ophthalmological fundus, electroretinogram (ERG), visual evoked potential (VEP) tests, and optic coherence tomography (OCT) and showed a bilateral defect of the optic nerves (Figure S1B). Magnetic resonance imaging (MRI) of cerebral and temporal bones did not reveal any abnormalities in supra-tentorial regions, posterior fossa, or inner ears (data not shown) in any index cases. Subjects 1–5 and 7–8 had isolated sensorial neurologic defects. Bilateral retinitis pigmentosa was diagnosed in subject 6 at 2 years of age because of low vision and nystagmus. ERG waves were indiscernible, and the fundus was altered. At the age of 20, his neurologic

[1]UMR 1163, Université Paris Descartes, Sorbonne Paris Cité, Institut IMAGINE, 24 Boulevard du Montparnasse, 75015 Paris, France; [2]Service de Génétique Médicale, Hôpital Purpan, 40031 Toulouse, France; [3]Institute for Integrative Biology of the Cell, Commissariat à l'Energie Atomique, Centre National de la Recherche Scientifique, Université Paris-Sud, Université Paris-Saclay, 91198, Gif-sur-Yvette Cedex, France; [4]UMRS 1120, Institut de la Vision, 75012 Paris, France; [5]Laboratory of Molecular and Cellular Screening Processes, Center of Biotechnology of Sfax, 1177 Sfax, Tunisia; [6]Service d'Oto-Rhino-Laryngologie, Hôpital Pitié-Salpêtrière, Assistance Publique–Hôpitaux de Paris, 75013 Paris, France; [7]Service d'Ophtalmologie, Hôpital Rangueil, 40031 Toulouse, France; [8]Service d'Ophtalmologie, Hôpital Pitié-Salpêtrière, Assistance Publique–Hôpitaux de Paris, 75013 Paris, France; [9]Service d' d'Oto-Rhino-Laryngologie, Hôpital Lariboisière, 75475 Paris, France; [10]Département de Génétique, Hôpital Pitié-Salpêtrière, Assistance Publique–Hôpitaux de Paris, 75013 Paris, France; [11]Service de Génétique, Laboratoire de Génétique Moléculaire, Hôpital Necker-Enfants Malades, Assistance Publique–Hôpitaux de Paris, 75015 Paris, France; [12]Centre de Référence des Surdités Génétiques, Service de Génétique, Hôpital Necker–Enfants Malades, Assistance Publique–Hôpitaux de Paris, 75015 Paris, France; [13]Service de Génétique, Hôpital Necker–Enfants Malades, Assistance Publique–Hôpitaux de Paris, 75015 Paris, France
[14]These authors have equally contributed to this research
*Correspondence: sandrine.marlin@aphp.fr
http://dx.doi.org/10.1016/j.ajhg.2017.09.007.

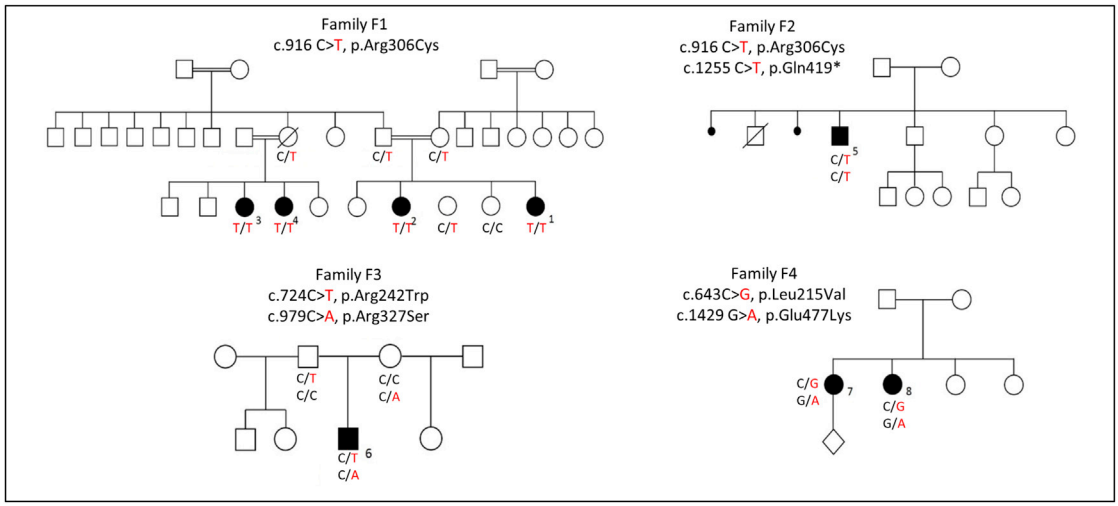

Figure 1. Pedigree of the Investigated Families
FDXR variants are reported according to GenBank: NM_024417.4.

examination showed only hypopallesthesia of the lower limbs. His cerebral MRI spectroscopy study and electromyogram were normal at this age.

None of the index cases (subjects 1 and 5–7) harbored mutations in *OPA1*, *TMEM126A,* or mitochondrial DNA. Molecular analysis of 35 different genes involved in severe congenital retinitis pigmentosa did not identify any causative variation. Because of a high degree of consanguinity in family 1 and the absence of disease in any parent, autosomal-recessive inheritance was hypothesized, and whole-exome-sequencing (WES) for subjects 1 and 3 was performed. Informed consent for diagnostic and research studies was obtained for all subjects in accordance with the Declaration of Helsinki protocols, and the local institutional review boards in Paris (Comité de Protection des Personnes, Ile de France II) approved the study.

DNA was extracted from leucocytes. Exome capture was performed with the Sure Select Human All Exon kit (Agilent Technologies). Agilent Sure Select Human All Exon (58 Mb, V6) libraries were prepared from 3 μg of genomic DNA sheared with an Ultrasonicator (Covaris) as recommended by the manufacturer. Barcoded exome libraries were pooled and sequenced with a HiSeq2500 system (Illumina), generating paired-end reads. After demultiplexing, sequences were mapped on the human genome reference (NCBI build 37, hg19 version) with BWA. Variant calling was carried out with the Genome Analysis Toolkit (GATK), SAMtools, and Picard tools. Single-nucleotide variants were called with GATK Unified Genotyper, whereas indel calls were made with the GATK IndelGenotyper_v2. All variants with a read coverage $\leq$2× and a Phred-scaled quality $\leq$20 were filtered out. All the variants were annotated and filtered with PolyWeb, an in-house-developed annotation software. For subject 1's library, a 86× mean depth of coverage was obtained, and 86% of the targeted exonic bases were covered by at least 15 independent sequencing reads (86% at 15×). The mean depth of coverage obtained for the exome library of subject 3 was 106×, and >97% of the targeted exonic bases were covered by at least 15 independent sequencing reads (>97% at 15×). Variant-filtering strategies and familial segregation led to the identification of only one homozygous variant shared by subjects 1 and 3 in *FDXR* (NM_024417.4): c.916C>T (p.Arg306Cys). This allele has been reported with a frequency of 8.85×10^{-6}, 1/112999 alleles (ExAc Browser Beta). We detected the *FDXR* c.916C>T homozygous variation in subjects 1–4 by Sanger sequencing (Figure S2). This variation co-segregated with the disease as expected for autosomal-recessive inheritance (Figure 1). We subsequently performed *FDXR* Sanger sequencing in subjects 5–8. Subject 5 was found to be compound heterozygous for the same c.916C>T *FDXR* variation and for c.1255C>T (p.Gln419*). Unfortunately, we did not have access to DNA of other members of this family. Subject 6 had two compound heterozygous missense variations: c.724C>T (p.Arg242Trp) and c.979C>A (p.Arg327Ser) (Figure 1 and Figure S2). Subjects 7 and 8 were found to be compound heterozygous for two other missense mutations, c.643C>G (p.Leu215Val) and c.1429G>A (p.Glu477Lys) (Figure 1 and Figure S2). DNA of other family members was not available. The pathogenicity clues for these *FDXR* variations are presented in Table 1. No *FDXR* mutation could be found in 12 independent subjects who demonstrated hearing loss due to a cochlear defect and optic atrophy, 12 subjects with isolated auditory neuropathy, 58 subjects with isolated optic atrophy, or four subjects with auditory neuropathy associated with peripheral neuropathy.

FDXR (OMIM 103270) encodes a mitochondrial NADPH: adrenodoxin oxidoreductase or ferredoxin reductase, the sole human ferredoxin reductase involved in the biosynthesis of iron-sulfur (Fe-S) clusters and heme formation.[6–8] We built a structural-homology model of ferredoxin reductase on the basis of the crystal structure of

Please cite this article in press as: Paul et al., *FDXR* Mutations Cause Sensorial Neuropathies and Expand the Spectrum of Mitochondrial Fe-S-Synthesis Diseases, The American Journal of Human Genetics (2017), http://dx.doi.org/10.1016/j.ajhg.2017.09.007

Table 1. Clinical Data of Affected Individuals and *FDXR* Genotypes

Families	F1				F2	F3	F4	
Familial origin	Tunisia				Algeria	France	Russia and Azerbaijan	
Individuals	1	2	3	4	5	6	7	8
Genders	F	F	F	F	M	M	G	G
Onset of hearing defect	13 yr	13 yr	15 yr	11 yr	teenage	20 yr	17y	5y
Hearing phenotype	BAN	BAN	BAN	BAN	BAN	BAN	BAN	BAN
Onset of visual defect	13 y	13y	36y	31y	31y	2 and 20y	Childhood	17y
Visual phenotype	BOA	BOA	infraclinical BOA	infraclinical BOA	infraclinical BOA	BRP and BOA	BOA	BOA
FDXR variations	c.916 C>T Ho	c.916 C>T Ho	c.916 C>T Ho	c.916 C>T Ho	c.916 C>T c.1255 C>T	c.724C>T, c.979C>A	c.643C>G, c.1429 G>A	c.643C>G, c.1429 G>A
Protein change	p.Arg306Cys	p.Arg306Cys	p.Arg306Cys	p.Arg306Cys	p.Arg306Cys, p.Gln419*	p.Arg242Trp, p.Arg327Ser	p.Leu215Val, p.Glu477Lys	p.Leu215Val, p.Glu477Lys
ExAC browser allele frequency	8.85×10^{-6}	8.85×10^{-6}	8.85×10^{-6}	8.85×10^{-6}	8.85×10^{-6} 0	0	0	0
Score prediction, SIFT	0.585	0.585	0.585	0.585	0.04 NA	0 0.3	0 0.03	0 0.03
Score prediction, Mutation Taster	1	1	1	1	1 NA	1 1	1 1	1 1

F1–4: families 1–4. M: male. F: female. BAN: bilateral auditory neuropathy. BOA: bilateral optic atrophy. BRP: bilateral retinitis pigmentosa. Ho: homozygous. NA: not available.

Bos taurus ferredoxin reductase (Figure 2A). This in silico modeling showed that the amino acids modified by the mutations are scattered in various parts of the protein but are not located in FAD or Fe-S binding sites. Three amino acid changes are predicted to create new H bonds: p.Leu215Val with Ala211 and Leu212, p.Arg242Trp with Leu279, and p.Arg327Ser with Gln313 (Figures 2B, 2C, and 2E). On the contrary, p.Arg306Cys is predicted to abolish the H bond with Glu349 (Figure 2D). These modifications are thus expected to destabilize ferredoxin reductase. Indeed, immunoblot analyses showed a major decrease of ferredoxin reductase in fibroblasts of subjects 1 and 5 (Figure 3A). To assess the consequences of *FDXR* mutations on ISC synthesis, we measured in-gel activity of mitochondrial and cytosolic aconitase, both containing ISC, that were found to be decreased (Figure 3B). Moreover, the amounts of heme oxygenase (HO-1) (Figure 3B) and SDHB, an iron-sulfur cluster (ISC)-containing subunit of respiratory chain complex II (Figure 3D), were severely decreased in subjects' fibroblasts. Finally, we also observed decreased activities of complexes I and III in these cells (Table 2). No fibroblasts were available for other affected subjects.

Several mitochondrial proteins are involved in ISC assembly; these include frataxin, encoded by *FXN* (MIM: 606829), the mutations of which result in Friedreich ataxia.[11] In yeast, Arh1 and Yfh1, the orthologs of human ferredoxin reductase and frataxin (FXN), respectively, are two factors involved in the first step of ISC assembly. Considering that (1) human *FXN* mutations induce mitochondrial iron accumulation and decreased activity of ISC enzymes,[8,12] (2) yeast Yfh1 defects result in mitochondrial iron overload,[13] and (3) yeast Arh1 defects induce a cellular iron uptake and disturbed iron trafficking within the cell,[14] we examined iron homeostasis in fibroblasts of subjects with *FDXR* mutations. Iron enters cells either via internalization of transferrin (Tf)-bound iron by transferrin receptor 1 (TfR1)-mediated endocytosis or by non-Tf-bound iron (NTBI) uptake.[15,16] An increase of the TfR1 steady-state level was observed in the fibroblasts of subjects 1 and 5 compared to control (187% and 184% of the control amount, respectively), and highly elevated amounts of mitochondrial superoxide dismutase 2 (SOD2) were also observed (Figure 3A and Figure S3). In keeping with this, increased mitochondrial superoxide production in S1 and S5 fibroblasts was detected by flow cytometry with MitoSOX (Figure 3C). These results suggest that mutations in the gene encoding ferredoxin reductase induce abnormal iron uptake by TfR1 and that they result in a major oxidative stress in mitochondria. Homeostasis of cellular iron is regulated by a post-transcriptional mechanism that involves iron-regulatory proteins (IRPs) and that modulates TfR1 levels, so that iron uptake does not take place in high-iron conditions. When grown for 3 days in low-iron conditions (fetal beef serum [FBS]-free DMEM, i.e., devoid of Tf-bound iron), a major increase in the ferritin steady-state level was observed in cultured fibroblasts of subject 1 and to a lesser extent those of subject 5 (Figure 3D and Figure S3), reflecting iron overload. Ferric ammonium citrate (FAC) is a soluble form of iron known to

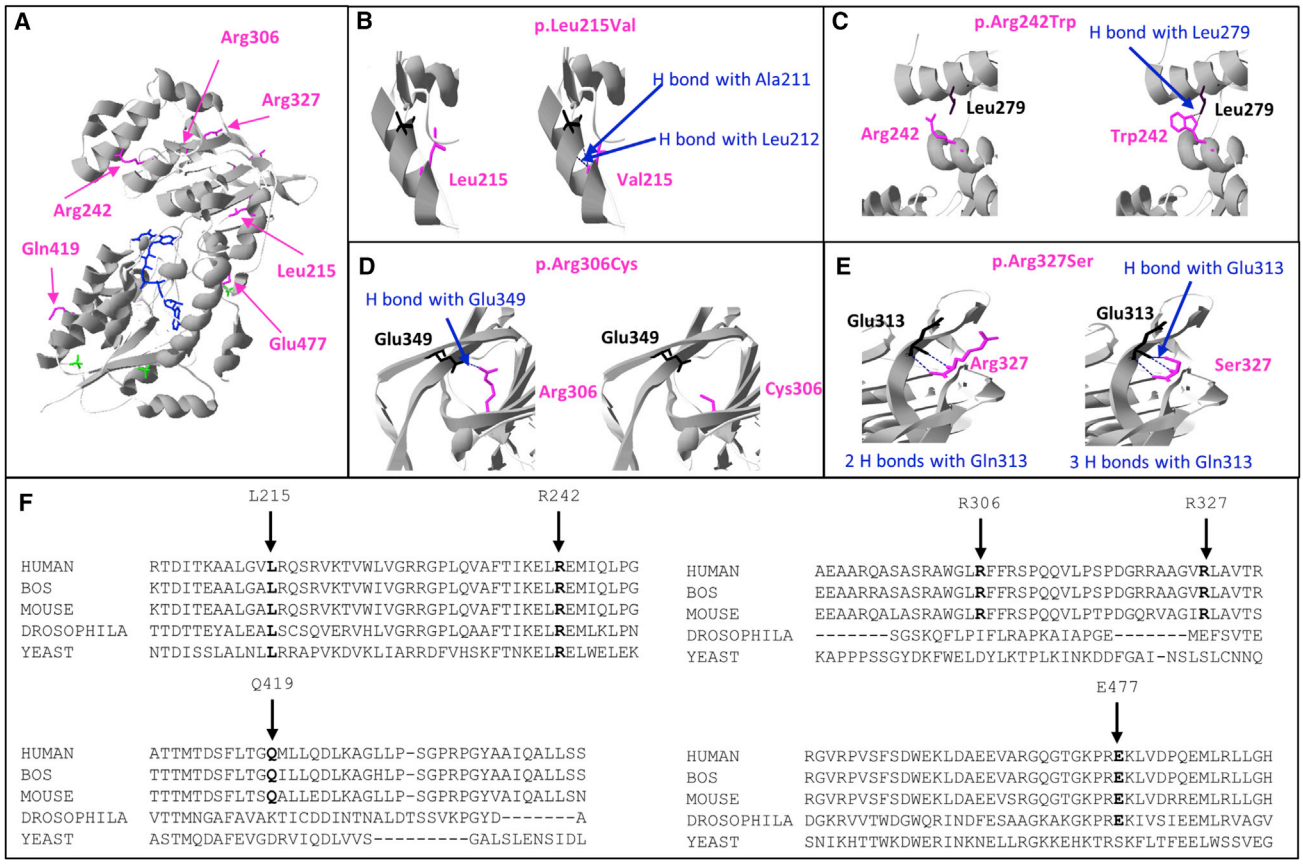

Figure 2. Ferredoxin Reductase Mutations
(A) Three-dimensional representation of the crystal structure of beef ferredoxin reductase (PDB: 1CJC). Blue and green sticks illustrate flavin adenine dinucleotide and sulfate ion, respectively. The mutated residues are highlighted in pink.
(B–E) H-bond modification resulting from p.Leu215Val, p.Arg242Trp, p.Arg306Cys, and p.Arg327Ser changes.
(F) Sequence alignment of ferredoxin proteins from various species. The arrows indicate the amino acid changes.

enhance NTBI uptake in fibroblasts[17] by a poorly understood mechanism that might involve the endocytic pathway.[16] After 3 days of incubation with FAC, control cells increased amounts of ferritin as expected, but S1 and S5 fibroblasts displayed a much higher ferritin steady-state level, showing that both fibroblast cultures abnormally increased their iron content (Figure 3D and Figure S3). As expected, in high-iron conditions, amounts of ACO1 (also called IRP1) decreased in control and subjects' fibroblasts, and amounts of TfR1 decreased in control cells. Cultured fibroblasts of subject 5 also had decreased amounts of TfR1 in high-iron conditions, but not only did TfR1 amounts fail to decrease in S1 fibroblasts, they actually increased, allowing abnormal iron uptake. We therefore quantified iron content in fibroblasts. When grown in low-iron conditions (no FAC and no FBS), control and affected individual fibroblasts showed a similar amount of iron. After a 3 day incubation with FAC, *FDXR* mutant fibroblasts exhibited a major increase in cellular iron content (a 50- and 100-fold change for S5 and S1, respectively), whereas control fibroblasts displayed a 2- to 3-fold upregulation (Figure 3E and Figure S3). Accordingly, SOD1 and SOD2 increased in high-iron conditions, reflecting the oxidative stress induced by iron overload. Nevertheless, mitochondrial ROS production was not modified in high- versus low-iron conditions (Figure 3C), suggesting that SOD2 induction efficiently protects against ROS overproduction. The mitochondrial

Table 2. Respiratory-Chain Enzyme Activities in Cultured Skin Fibroblasts

	S1	S5	C
Absolute Activities (nmol/min/mg protein)			
CI	**7**	**6**	14 ± 3
CII	29	26	22 ± 2
CIII	**82**	**125**	190 ± 23
CIV	**61**	144	107 ± 14
CV	**10**	14	21 ± 3
Activity Ratios			
CI/CII	**0,23**	**0,22**	0,57 ± 0,11
CIII/CII	**2,9**	**4,9**	8,8 ± 0,8
CIV/CII	**2,1**	5,7	4,7 ± 0,5
CV/CII	**0,34**	0,56	0,87 ± 0,09

CI–V: complexes I–V. Abnormal values are shown in bold.

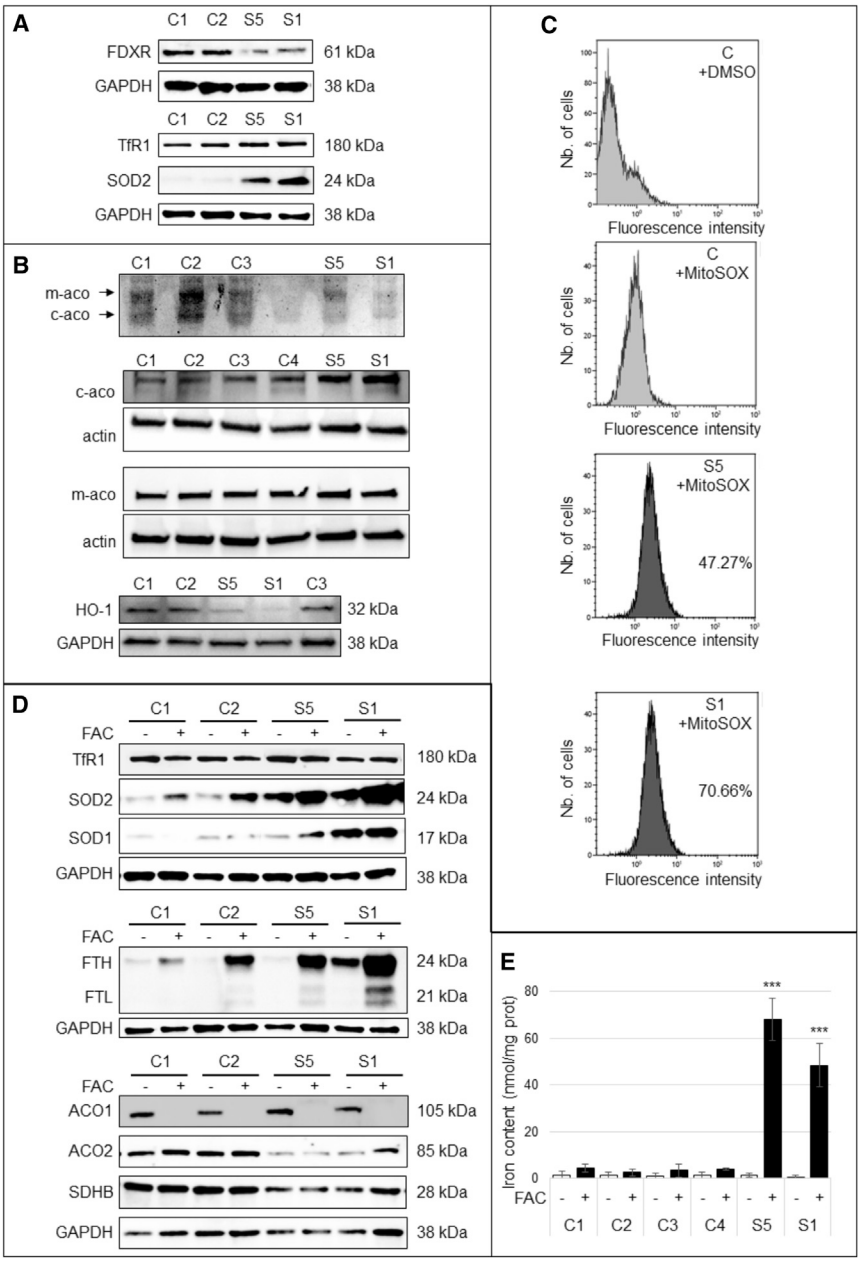

Figure 3. A Defect in Ferredoxin Reductase Results in Deregulation of Iron Homeostasis

(A) Decreased steady-state levels of ferredoxin reductase (upper panel) and increased steady-state levels of TfR1 and SOD2 (lower panel) in fibroblasts of subjects 1 and 5 (S1, S5). Controls (C1 and C2) are representative of three controls. Fibroblasts were grown in DMEM with 10% FBS. Ferredoxin reductase was studied in reducing conditions, and SOD2 and TfR1 were studied in non-reducing conditions so that TfR1 dimerization would be maintained. GAPDH was used as a loading control.

(B) Upper panel: in-gel aconitase assays revealed decreased mitochondrial (m-aco) and cytosolic (c-aco) aconitases in S1 and S5 fibroblasts compared to controls (C1–3).[9] Lower panel: decreased HO-1 steady-state levels in S1 and S5 fibroblasts. C1–3: controls 1–3.

(C) Measurement of mitochondrial reactive oxygen species (ROS). Fibroblasts were grown in low- (-FAC) or high- (+FAC) iron conditions, and ROS amounts were similar in both conditions for control (C is representative of three controls) and subjects 1 and 5. The figure presents the ROS content in high-iron conditions. The numbers represent the percent of fluorescence intensity of subjects' fibroblasts compared to controls. ROS were measured as previously described.[10]

(D) Steady-state levels of proteins involved in iron homeostasis. TfR1, SOD1, and SOD2 were studied in non-reducing conditions, ferritin (FTH, FTL), ACO1, ACO2, and SDH were studied in reducing conditions in controls (C1–2), and FDXR fibroblasts grown in FBS-free DMEM medium were studied in low (-FAC) and high- (+FAC) iron conditions. GAPDH was used as a loading control.

(E) Iron quantification using the ferrozine-based colorimetric assay in fibroblasts of controls (C1–C4) and FDXR subjects (S1, S5) grown in FBS-free DMEM medium and low- (-FAC) or high- (+FAC) iron conditions. The data are the means ± SEM of three independent experiments. A Student-Newman-Keuls ANOVA multifactorial test was used. ***$p < 0.001$.

We harvested cultured skin fibroblasts on ice by scraping cells in reducing (2 μM DTT, denaturation at 95°C for 5 min) or non-reducing (no DTT, no heat denaturation) cell lysis buffer. SDS-PAGE was performed on whole-cell protein extracts in 10% or 7.5% acrylamide gel for reducing and non-reducing conditions, respectively. Immunodetections were performed in PBS with 5% milk and 0.05% Tween 20 (SIGMA) and the following antibodies: mouse anti-TfR1 (ab108985), rabbit anti-ferritin (ab75973), rabbit anti-FDXR (ab204310), rabbit anti-HO1 (Enzo Life Sciences, ADI-SPA-896), mouse anti-SOD1 (ab86454), mouse anti-SOD2 (ab125702), rabbit anti-GAPDH (ab62489), rabbit anti-ACO1 (ab126595), rabbit anti-ACO2 (ab129069). HRP-conjugated goat anti-mouse IgG H&L (ab6789), or goat anti-rabbit IgG (ab6721) were used as secondary antibodies before ECL-based detection (SuperSignal[18] West Dura, Thermo Scientific). Images were visualized on a CCD camera (BioRad) and analyzed with ImageLab software (BioRad).

aconitase (ACO2) and SDHB amounts were decreased in subjects' fibroblasts in low- and high-iron conditions because of the ISC defect induced by *FDXR* mutations. Altogether, these results suggest that the defect in ferredoxin reductase induced a failure to repress iron uptake, as previously demonstrated in *FDXR* knock-down human cells[18] and in *ARH1*-deficient yeast cells.[14]

To definitively demonstrate the pathogenic nature of the identified *FDXR* mutations, we studied their effect on the growth of a *Saccharomyces cerevisiae* strain in which *ARH1* was deleted. Yeast mitochondrial Arh1 shares 35% identity with ferredoxin reductase (Figure 2F) and is essential for cell viability. Consistent with previous studies,[19] the *ARH1*-null mutation (*arh1Δ*) led to lethality that was rescued

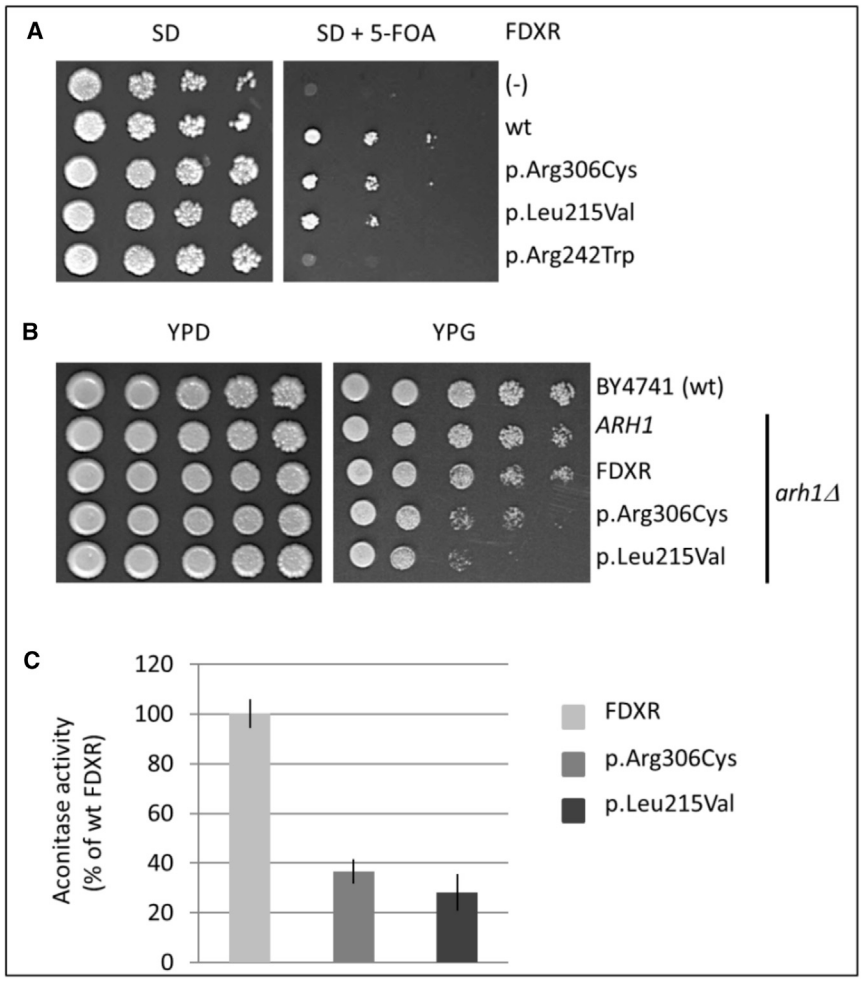

Figure 4. Functional Complementation Assay of the Yeast *arh1Δ* Mutant Strain Expressing Either the Wild-Type *FDXR* or the *FDXR* Mutants

(A) Growth on synthetic dextrose (SD) with or without 5-fluoroorotic acid (5-FOA) of *arh1Δ* and not D cells expressing the yeast wild-type *ARH1* and transformed with the wild-type *FDXR* (wt), the *FDXR* mutants, or the corresponding empty plasmid (-) under the control of the strong PGK promoter. 5-FOA treatment, as described by Boeke,[20] eliminates the plasmid encoding the yeast *ARH1* and allows one to evaluate growth capability of the *arh1Δ* cells expressing only *FDXR* or its mutated forms.

(B) Growth after 5-FOA treatment of wt cells (BY4741) and *arh1Δ* cells expressing wt*ARH1*, *FDXR*, or the *FDXR* mutants. Cells were spotted onto fermentable (YPD) or non-fermentable (YPG) plates. Drop dilution growth tests were performed at 1/10 dilution steps, and plates were incubated for 3 days at 28°C.

(C) *FDXR* mutations affect aconitase activity. Aconitase assays on crude yeast extracts from *arh1Δ* cells expressing the wild-type *FDXR* (wt) or the mutant forms Arg306Cys and Leu215Val are shown. Cells were grown to mid-logarithmic phase, and total crude extracts were prepared and analyzed for aconitase activity as previously described.[21] Consumption of *cis*-aconitate was monitored spectrophotometrically at 240 nm at a molar absorption of 3,600 $M^{-1} \times cm^{-1}$. Activities shown are an average of two independent experiments. Error bars indicate SD.

by overexpression of *ARH1* (Figures 4A and 4B). Using a well-known plasmid-shuffling system,[20] we found, contrary to findings of the Manzella study,[19] that overexpression of wild-type (wt) human *FDXR* cDNA was able to rescue *arh1Δ* lethality (Figures 4A and 4B), demonstrating that *FDXR* is the true functional ortholog of *ARH1*, as suggested by Webert et al.,[22] who used purified human ferredoxin reductase instead of Arh1 in an *in vitro* reconstitution of yeast Fe/S cluster synthesis on Isu1. Subsequently, we introduced amino acid changes into the ferredoxin reductase sequence for 3/5 missense mutations. p.Arg242Trp was completely unable to complement the *arh1Δ* growth defect (Figure 4A), indicating that this mutation disrupts the ferredoxin reductase function. p.Arg306Cys and p.Leu215Val changes did not modify cell growth in this condition but induced a growth defect on non-fermentable (respiratory) substrate (YPG, Figure 4B). Because *Arh1* is required for ISC assembly, we further measured the enzyme activity of mitochondrial aconitase, which contains an ISC. Spectrophotometric analyses revealed that aconitase activity in *arh1Δ* cells expressing p.Arg306Cys and p.Leu215Val was decreased in comparison to that in cells expressing WT *Fdxr* (Figure 4C), thus confirming the deleterious nature of the *FDXR* variants.

By using exome sequencing, we found mutations in the gene encoding the mitochondrial ferredoxin reductase in eight subjects from four independent families, and functional studies in yeast clearly established that the variations tested cause disease in these subjects. Mutations in several genes involved in ISC assembly have been reported in human diseases (Friedreich ataxia due to *FXN* mutations is the most frequent).[11] These mutations result in a wide panel of variably severe clinical presentations, ranging from fatal infantile leukodystrophy to mitochondrial myopathy.[23] Interestingly, whereas mutations in *FDX1L*, encoding ferredoxin-2 (FDX2), result in mitochondrial myopathy and myoglobinuria,[24] we showed here that mutations in the gene encoding its reductase (FDXR) result in sensorial neuropathies. Those points highlight the wide clinical heterogeneity of mitochondrial disorders even when the disease-causing mutations arise in a same pathway. Ferredoxin reductase is also able to reduce ferredoxin-1 (FDX1), which is not involved in ISC assembly but rather in steroid metabolism. Nevertheless, none of the subjects with *FDXR* mutations show any defect in steroid metabolism, suggesting that these specific mutations do not modify FDX1 function or steroid metabolism. Why *FDXR* mutations result in sensorial neuropathies is

intriguing, and further studies will be needed to help us understand it. Nevertheless, several examples of isolated deafness or optic atrophy have been described in mitochondrial disorders and result from mitochondrial DNA mutations (m.1555A>G)[25] or nuclear gene mutations, such as *OPA1*[21] and *PNPT1*.[26]

Indirect evidence of mitochondrial iron overload in *arh1Δ* yeast cells expressing human mutant proteins is provided by increased SOD2 levels and defective mitochondrial aconitase activity. Moreover, we detected a major iron overload and increased mitochondrial ROS production in fibroblasts of affected individuals, which is in accordance with previous studies performed in human FDXR-knockdown cells[18] as well as *FDX2*-knockdown cells.[27] We also observed increased TfR1 amounts that could be ascribed to the increased binding of IRP1 to the iron-responsive element; this increased binding activity was induced by an ISC defect, as previously demonstrated.[18,27] Finally, we detected a considerable amount of iron in *FDXR* mutant cells when we grew these in high-iron conditions, suggesting that these cells are unable to regulate iron entry. Nevertheless, ferritin is not repressed in *FDXR* mutant fibroblasts, suggesting that an additional defect of iron homeostasis could occur in cultured skin fibroblasts.

In conclusion, we have shown that biallelic mutations in *FDXR* lead to sensorial neuropathies, confirming the critical role of the Fe-S biogenesis in the function of optic and auditory neurons.

Supplemental Data

Supplemental Data contain phenotype descriptions (Supplemental Note), clinical investigations, *FDXR* sequencing, and immunoblotting quantification data and can be found with this article online at http://dx.doi.org/10.1016/j.ajhg.2017.09.007.

Acknowledgments

We acknowledge the parents, the patients, and the physicians for their participation; Institut IMAGINE and the association S'entendre for their support; and Dr. Patrizia Amati Bonneau for *OPA1* and *TMEM126A* studies. This work was partially funded through the E-Rare project GENOMIT (01GM1207) and the Agence Nationale de la Recherche (ANR-10-IAHU-01). A.D. was supported by a fellowship from ApoPharma.

Received: February 10, 2017
Accepted: September 11, 2017
Published: September 28, 2017

Web Resources

UCSC genome browser, https://genome.ucsc.edu/
ExAC Browser, http://exac.broadinstitute.org/
Online Mendelian Inheritance in Man (OMIM), https://www.ncbi.nlm.nih.gov/omim
Ensembl database, http://www.ensembl.org/index.html
Saccharomyces genome database, http://www.yeastgenome.org/
Basic local alignment search tool (Blast), https://blast.ncbi.nlm.nih.gov/Blast.cgi
Expression atlas, http://www.ebi.ac.uk/gxa/

References

1. Nikolopoulos, T.P. (2014). Auditory dyssynchrony or auditory neuropathy: understanding the pathophysiology and exploring methods of treatment. Int. J. Pediatr. Otorhinolaryngol. *78*, 171–173.
2. Moser, T., and Starr, A. (2016). Auditory neuropathy–neural and synaptic mechanisms. Nat. Rev. Neurol. *12*, 135–149.
3. Bocquet, B., Lacroux, A., Surget, M.O., Baudoin, C., Marquette, V., Manes, G., Hebrard, M., Sénéchal, A., Delettre, C., Roux, A.F., et al. (2013). Relative frequencies of inherited retinal dystrophies and optic neuropathies in Southern France: assessment of 21-year data management. Ophthalmic Epidemiol. *20*, 13–25.
4. Namba, K., Mutai, H., Takiguchi, Y., Yagi, H., Okuyama, T., Oba, S., Yamagishi, R., Kaneko, H., Shintani, T., Kaga, K., and Matsunaga, T. (2016). Molecular impairment mechanisms of novel OPA1 mutations predicted by molecular modeling in patients with autosomal dominant optic atrophy and auditory neuropathy spectrum disorder. Otol. Neurotol. *37*, 394–402.
5. Meyer, E., Michaelides, M., Tee, L.J., Robson, A.G., Rahman, F., Pasha, S., Luxon, L.M., Moore, A.T., and Maher, E.R. (2010). Nonsense mutation in TMEM126A causing autosomal recessive optic atrophy and auditory neuropathy. Mol. Vis. *16*, 650–664.
6. Ewen, K.M., Kleser, M., and Bernhardt, R. (2011). Adrenodoxin: the archetype of vertebrate-type [2Fe-2S] cluster ferredoxins. Biochim. Biophys. Acta *1814*, 111–125.
7. Jung, Y.S., Gao-Sheridan, H.S., Christiansen, J., Dean, D.R., and Burgess, B.K. (1999). Purification and biophysical characterization of a new [2Fe-2S] ferredoxin from Azotobacter vinelandii, a putative [Fe-S] cluster assembly/repair protein. J. Biol. Chem. *274*, 32402–32410.
8. Stehling, O., Wilbrecht, C., and Lill, R. (2014). Mitochondrial iron-sulfur protein biogenesis and human disease. Biochimie *100*, 61–77.
9. Shi, Y., Ghosh, M.C., Tong, W.-H., and Rouault, T.A. (2009). Human ISD11 is essential for both iron-sulfur cluster assembly and maintenance of normal cellular iron homeostasis. Hum. Mol. Genet. *18*, 3014–3025.
10. Mukhopadhyay, P., Rajesh, M., Haskó, G., Hawkins, B.J., Madesh, M., and Pacher, P. (2007). Simultaneous detection of apoptosis and mitochondrial superoxide production in live cells by flow cytometry and confocal microscopy. Nat. Protoc. *2*, 2295–2301.
11. Campuzano, V., Montermini, L., Moltò, M.D., Pianese, L., Cossée, M., Cavalcanti, F., Monros, E., Rodius, F., Duclos, F., Monticelli, A., et al. (1996). Friedreich's ataxia: autosomal recessive disease caused by an intronic GAA triplet repeat expansion. Science *271*, 1423–1427.
12. Schmucker, S., Argentini, M., Carelle-Calmels, N., Martelli, A., and Puccio, H. (2008). The in vivo mitochondrial two-step maturation of human frataxin. Hum. Mol. Genet. *17*, 3521–3531.
13. Adamec, J., Rusnak, F., Owen, W.G., Naylor, S., Benson, L.M., Gacy, A.M., and Isaya, G. (2000). Iron-dependent self-assembly

of recombinant yeast frataxin: implications for Friedreich ataxia. Am. J. Hum. Genet. *67*, 549–562.

14. Li, J., Saxena, S., Pain, D., and Dancis, A. (2001). Adrenodoxin reductase homolog (Arh1p) of yeast mitochondria required for iron homeostasis. J. Biol. Chem. *276*, 1503–1509.
15. Lane, D.J.R., Merlot, A.M., Huang, M.L., Bae, D.H., Jansson, P.J., Sahni, S., Kalinowski, D.S., and Richardson, D.R. (2015). Cellular iron uptake, trafficking and metabolism: Key molecules and mechanisms and their roles in disease. Biochim. Biophys. Acta *1853*, 1130–1144.
16. Sohn, Y.-S., Ghoti, H., Breuer, W., Rachmilewitz, E., Attar, S., Weiss, G., and Cabantchik, Z.I. (2012). The role of endocytic pathways in cellular uptake of plasma non-transferrin iron. Haematologica *97*, 670–678.
17. Buys, S.S., Martin, C.B., Eldridge, M., Kushner, J.P., and Kaplan, J. (1991). Iron absorption in hypotransferrinemic mice. Blood *78*, 3288–3290.
18. Shi, Y., Ghosh, M., Kovtunovych, G., Crooks, D.R., and Rouault, T.A. (2012). Both human ferredoxins 1 and 2 and ferredoxin reductase are important for iron-sulfur cluster biogenesis. Biochim. Biophys. Acta *1823*, 484–492.
19. Manzella, L., Barros, M.H., and Nobrega, F.G. (1998). ARH1 of Saccharomyces cerevisiae: a new essential gene that codes for a protein homologous to the human adrenodoxin reductase. Yeast *14*, 839–846.
20. Boeke, J.D., Trueheart, J., Natsoulis, G., and Fink, G.R. (1987). 5-Fluoroorotic acid as a selective agent in yeast molecular genetics. Methods Enzymol. *154*, 164–175.
21. Delettre, C., Lenaers, G., Griffoin, J.M., Gigarel, N., Lorenzo, C., Belenguer, P., Pelloquin, L., Grosgeorge, J., Turc-Carel, C., Perret, E., et al. (2000). Nuclear gene OPA1, encoding a mitochondrial dynamin-related protein, is mutated in dominant optic atrophy. Nat. Genet. *26*, 207–210.
22. Webert, H., Freibert, S.A., Gallo, A., Heidenreich, T., Linne, U., Amlacher, S., Hurt, E., Mühlenhoff, U., Banci, L., and Lill, R. (2014). Functional reconstitution of mitochondrial Fe/S cluster synthesis on Isu1 reveals the involvement of ferredoxin. Nat. Commun. *5*, 5013.
23. Beilschmidt, L.K., and Puccio, H.M. (2014). Mammalian Fe-S cluster biogenesis and its implication in disease. Biochimie *100*, 48–60.
24. Spiegel, R., Saada, A., Halvardson, J., Soiferman, D., Shaag, A., Edvardson, S., Horovitz, Y., Khayat, M., Shalev, S.A., Feuk, L., and Elpeleg, O. (2014). Deleterious mutation in FDX1L gene is associated with a novel mitochondrial muscle myopathy. Eur. J. Hum. Genet. *22*, 902–906.
25. Ruiz-Pesini, E., Lott, M.T., Procaccio, V., Poole, J.C., Brandon, M.C., Mishmar, D., Yi, C., Kreuziger, J., Baldi, P., and Wallace, D.C. (2007). An enhanced MITOMAP with a global mtDNA mutational phylogeny. Nucleic Acids Res. *35*, D823–D828.
26. von Ameln, S., Wang, G., Boulouiz, R., Rutherford, M.A., Smith, G.M., Li, Y., Pogoda, H.M., Nürnberg, G., Stiller, B., Volk, A.E., et al. (2012). A mutation in PNPT1, encoding mitochondrial-RNA-import protein PNPase, causes hereditary hearing loss. Am. J. Hum. Genet. *91*, 919–927.
27. Sheftel, A.D., Stehling, O., Pierik, A.J., Elsässer, H.P., Mühlenhoff, U., Webert, H., Hobler, A., Hannemann, F., Bernhardt, R., and Lill, R. (2010). Humans possess two mitochondrial ferredoxins, Fdx1 and Fdx2, with distinct roles in steroidogenesis, heme, and Fe/S cluster biosynthesis. Proc. Natl. Acad. Sci. USA *107*, 11775–11780.